PCCP

ROYAL SOCIETY OF CHEMISTRY

PAPER

Check for updates

Cite this: *Phys. Chem. Chem. Phys.*, 2023, **25**, 11130

Computational investigation of explicit solvent effects and specific interactions of hydroxypyrene photoacids in acetone, DMSO, and water†

Niklas Sülzner * and Christof Hättig

Received 20th February 2023,
Accepted 27th March 2023

DOI: 10.1039/d3cp00800b

rsc.li/pccp

This work employs the correlated wavefunction-based methods ADC(2) and CC2 in combination with the implicit solvent model COSMO to calculate the UV/Vis absorption and fluorescence emission energies of particularly strong hydroxypyrene photoacids in acetone. According to the Förster cycle, the electronic transition energies are first used to compute $\Delta pK_a = pK_a^* - pK_a$, *i.e.*, the pK_a change upon excitation and then the excited-state pK_a (labeled pK_a^*) with ground-state pK_a values based on COSMO-RS as additional inputs. Furthermore, for the strongest photoacid of that class, namely tris(1,1,1,3,3,3-hexafluoropropan-2-yl)-8-hydroxypyrene-1,3,6-trisulfonate, the need to go beyond implicit solvation and to account for explicit solvent effects on the electronic transition energies and the resulting ΔpK_a is investigated in the solvents acetone, dimethyl sulfoxide (DMSO), and water. For this, a hybrid implicit–explicit approach is followed by comparing micro-solvated structures that are generated based on Kamlet–Taft considerations. While implicit solvent effects are mostly sufficient for the aprotic solvent acetone, one explicit solvent molecule seems relevant for DMSO due to its stronger hydrogen-bond (HB) acceptance and hence larger interaction with the photoacid OH group as a HB donor. For the protic solvent water, the situation is more complicated, involving at least one water molecule at the OH group and up to three water molecules at the O^- group of the corresponding base. Finally, these results are used to rationalize the experimentally observed spectral evolution of the photoacid absorption band in acetone–water solvent mixtures.

1. Introduction

Proton transfer (PT) is omnipresent in chemistry and its related fields, including countless examples from biochemistry, chemical synthesis, and (acid–base) catalysis, as well as industrial applications.[1–3] Proton transfer can also take place in an electronically excited state, referred to as excited-state proton transfer (ESPT), *e.g.*, as observed in nature for the chromophores of the green fluorescent protein[4,5] and fireflys D-Luciferin,[6,7] or the anthocyanin pigments in plants.[8,9]

Owing to this fundamental importance, there has been a huge interest in the study of proton-transfer reactions since the beginnings of chemistry, both with respect to the underlying thermodynamics as well as the kinetics.[10,11] From a thermodynamic perspective, the acid dissociation constant K_a or the pK_a, *i.e.*, its negative decadic logarithm, is the most important quantity as it quantifies the Brønsted acid strength.[12] Nowadays, there is a broad variety of available methods, both experimentally and computationally, for the determination of pK_a in aqueous and non-aqueous solutions.[13–15]

Regarding the kinetics, a molecular probe is typically required to experimentally obtain information on the PT mechanisms including relevant intermediates as well as rate constants for the individual steps. For this task, so-called photoacids have been established as particularly powerful tools during the last decades (*vide infra*). Photoacids are molecules that exhibit an increase in acidity (*i.e.*, a decrease in pK_a) upon electronic excitation.[16,17] Thus, the excited-state pK_a (from now on referred to as pK_a^*) is smaller than the ground-state pK_a. As a consequence, photo-excitation can trigger an ESPT[18] from the photoacid to a nearby proton acceptor, *e.g.*, the solvent or any other Brønsted base.[19] In particular, the use of pulsed lasers has made it possible to temporally initiate the ESPT event, which conveniently allows to investigate the associated

Lehrstuhl für Theoretische Chemie, Ruhr-Universität Bochum, 44780 Bochum, Germany. E-mail: niklas.suelzner@rub.de; Fax: +49 (0)234 32-14045; Tel: +49 (0)234 32-24250

† Electronic supplementary information (ESI) available: First electronic transition energies of photoacid **B** for different combinations of methods for geometries and electronic excitations; numerical absorption and emission energies of the acid and base of the six photoacids in implicit acetone; ΔpK_a values based on COSMO-CC2//COSMO-CC2; additional absorption and emission energies for different hydrogen-bonded complexes of photoacid **B** in acetone. See DOI: https://doi.org/10.1039/d3cp00800b

This journal is © the Owner Societies 2023

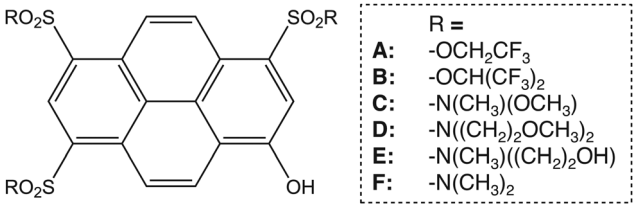


Fig. 1 Molecular structures of the hydroxypyrene photoacids studied in the current work. Compound **F** is also known as HPTA (8-hydroxy-*N*,*N*,*N*′,*N*′,*N*″,*N*″-hexamethylpyrene-1,3,6-trisulfonamide).

dynamics in real time with time-resolved spectroscopy.[20,21] Other applications of photoacids include their use as proton sources for (photo)catalysis,[22,23] as pH-dependent imaging agents in biological cells,[24,25] or for single-molecule microscopy.[26,27]

While most weak ($pK_a^* > 0$) photoacids like 8-hydroxypyrene-1,3,6-trisulfonate (HPTS or pyranine) are restricted to ESPT in neat water[28,29] or aqueous solutions containing an additional base[30] or co-solvent,[31–34] those with a negative pK_a^*, referred to as super-photoacids, can also perform an ESPT in other protic (*e.g.*, alcohols)[35,36] or even aprotic solvents such as dimethyl sulfoxide (DMSO).[37] Known classes of super-photoacids include cyanonaphthols,[38–40] *N*-substituted hydroxyquinolines,[41–44] cyanine dyes,[45–50] and naphthalimides.[51–54] Recently, Gregor Jung and co-workers introduced a new class of hydroxypyrene super-photoacids (see Fig. 1) by functionalizing the sulfonate groups of HPTS with highly electron-withdrawing ester (**A–B**) or amide (**C–E**) moieties.[55] Overall, the substitution does not significantly alter the pK_a drop upon excitation ($\sim$6 units), but allows to downshift the pK_a^* by up to 5 units by changing the ground-state pK_a, yielding a set of photoacids with pK_a^* between -0.8 and -3.9 (in water).

The solvatochromism in a broad range of 29 solvents[56] and the ESPT kinetics (on the ps–ns timescale) in DMSO[55] have been studied for the full set of these new photoacids (**A–E**). In addition, for photoacids **B** and **E**, the ESPT has been studied more thoroughly in water, methanol, and ethanol with ultrafast time-resolved fluorescence spectroscopy (sub-ps timescale).[57] Recently, the involvement of a hydrogen-bonded ion pair (HBIP) as a spectrally distinct species and intermediate in the excited state has been reported for the ESPT of photoacid **A** within a complex with tri-*n*-octylphosphine oxide (TOPO) in acetonitrile solution.[58,59]

Whereas most standard photoacids cannot transfer their proton to DMSO, the strongest super-photoacid **B** of that class, namely tris(1,1,1,3,3,3-hexafluoropropan-2-yl)-8-hydroxypyrene-1,3,6-trisulfonate ($pK_a^* \approx -4$ in water) had shown indications to do so even in acetone.[55] As an aprotic and only moderately basic solvent, acetone is a quite unusual medium for PT reactions. Most recently, the ESPT of photoacid **B** has been studied experimentally in acetone–water mixtures[60] and neat acetone.[61] The study in acetone–water mixtures showed that a reaction complex between the photoacid and water—formed either already in the ground state or directly after excitation—becomes crucial for the ESPT dynamics of photoacid **B** in these solvent mixtures.[60] In particular, association constants

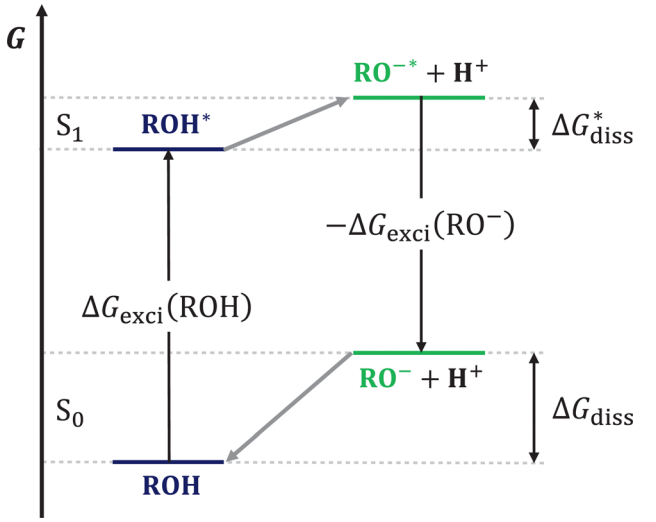


Fig. 2 Schematic illustration of the Förster cycle.

could be determined from the changes in the UV/Vis absorption spectra, but more detailed spectroscopic information on such intermediates was not directly accessible. Similarly, the study in neat acetone did not fully answer the question regarding the actual proton acceptor, keeping the possibility of ESPT to acetone still unsettled.[61]

In a previous computational study, we have applied the Förster cycle (Fig. 2) to determine the pK_a^* values of the photoacids **A–F** in the related solvent DMSO through the ground-state pK_a and electronic transition energies.[62] pK_a has been calculated using COSMO-RS (COSMO for real solvents),[63–66] while UV/Vis absorption and fluorescence emission energies have been computed using the wavefunction-based methods ADC(2) and CC2 in combination with the conductor-like screening model (COSMO).[66–68] To the best of our knowledge, that study has been the first that applied such higher-level electronic-structure methods to the study of photoacids, in general, and pK_a^*, in particular, apart from some studies by Aquino and co-workers on anthocyanins, also using ADC(2) but not considering pK_a^*.[69–73] However, the significant efforts to obtain pK_a^* at the TDDFT level, both directly using a thermodynamic cycle or approaches based on correcting ground-state pK_a values (like this work), should be noted as well.[74–81] Furthermore, that study (in DMSO) revealed some interesting insights into the origin of photoacidity of these systems, but fully remained within the implicit solvation picture, thus neglecting any explicit solvent effects on ΔpK_a.

In this work, we address these open questions from a computational perspective. The previous approach for the theoretical spectroscopy will be extended to the new target solvent acetone. The calculated pK_a in acetone based on recently determined linear free-energy relationship (LFER) parameters for COSMO-RS[82] in combination with ΔpK_a from calculated spectra will give access to the pK_a^* values of the photoacids **A–F** in acetone. These allow to judge and compare the thermodynamic possibility of ESPT of these different

compounds in acetone. Second, the need to go beyond implicit solvation by incorporating explicit solvent molecules in the first solvation shells in different solvent environments will be investigated. Here, the focus will be set to the additional effect of explicit solvent on the electronic excitation energies, which will also affect the calculated acidity increase upon excitation (ΔpK_a). Finally, the role of acetone and water as proton acceptors in acetone solution will be briefly compared by providing additional spectroscopic information on possible reaction complexes to complement the experimental studies.

2. Computational details

2.1 General information

All quantum-chemical calculations have been done using the TURBOMOLE program package (version 7.6).[83,84] The resolution-of-the-identity (RI) approximation was used in all MP2, ADC(2), and CC2 calculations with the ricc2 module. In addition, the frozen-core approximation was applied for the 1s orbitals at C, N, O, F and the 1s2s2p orbitals at S. To ensure convergence with diffuse basis functions, the integral screening threshold for the MO calculations (\$scftol) was lowered to 10^{-15}. Calculations in bulk solution refer to the implicit solvent model COSMO with values for the relative dielectric constant ε_r and refractive index n for the respective solvents: acetone (ε_r = 20.56, n = 1.359), DMSO (ε_r = 46.45, n = 1.479), and water (ε_r = 78.30, n = 1.333) at 25 °C (taken from ref. 56). Default COSMO parameters were used for the cavity construction. For the combination of COSMO with the methods ADC(2) and CC2 for electronic excitation energies, the post-SCF coupling scheme in the non-equilibrium solvation limit was used. Note that the post-SCF scheme, as first introduced in ref. 85 for Polarizable Embedding (PE) and later compared for COSMO[86] to other reaction schemes, does only include linear-response (LR) but no state-specific (SS) contributions. Although these could be added *via* corrected linear response (cLR), we anticipate only a small effect from SS because of large transition dipole moments of the relevant (first) electronic transitions studied here. The notation A//B is used for referring to an electronic excitation energy that was computed at a level A using a geometry optimized at a level B. All structures together with their Hartree–Fock energies are available in ref. 87.

2.2 Electronic transition energies

Ground-state (S_0) equilibrium geometries were optimized in the cc-pVDZ basis set[88,89] using MP2[90,91] or CC2[92] in the gas phase and COSMO-MP2[93] or COSMO-CC2[94] in solution with the ε_r values for the respective solvents as described above in the text. Similarly, geometries for the first excited state (S_1) were also optimized in the cc-pVDZ basis set, but using ADC(2)[92] or CC2[95] for the gas phase and only COSMO-ADC(2)[94] for the solution phase. If available, initial structures were taken from the previous calculations in DMSO (see ref. 62; therein available from ref. 96) and re-optimized in the target solvent (mostly acetone). At the final geometries, vertical electronic excitation energies were then calculated in the larger aug-cc-pVDZ basis set[89,97] with the desired method(s) ADC(2),[98] CC2,[99] COSMO-ADC(2),[94] or COSMO-CC2.[94] UV/Vis absorption was calculated at the S_0 equilibrium structures, while fluorescence emission was obtained at the S_1 equilibrium structures. As in the usual protocol for photoacidity,[55] also this study uses the absorption and emission energies to compute ΔpK_a values based on the Förster cycle (*cf.* Fig. 2), according to:

$$\Delta pK_a = pK_a^* - pK_a = \frac{\Delta G_{exci}(RO^-) - \Delta G_{exci}(ROH)}{RT\ \ln(10)}, \qquad (1)$$

with the excitation Gibbs free energies ΔG_{exci}(ROH) and $\Delta G_{exci}(RO^-)$ for the two species, the ideal gas constant R, and the absolute temperature T. These ΔG_{exci} values were approximated by the corresponding experimental or calculated UV/Vis absorption and fluorescence emission energies from S_0 to S_1 which is a bright ππ* transition. Since the excitation energy for S_1 is insensitive to conformational changes in the substituents of the sulfonate groups, these calculations have for each molecule only been done for the conformer with the lowest energy.

2.3 Ground-state and excited-state acidities

Ground-state pK_a values were calculated with COSMO-RS as implemented in COSMO*therm* (version 2021)[100] at the BP-TZVP and BP-TZVPD-FINE levels of theory. These calculations employ—in difference to those described in Section 2.2—geometries that are optimized with $\varepsilon_r = \infty$ for COSMO. Details on COSMO-RS itself,[63–66,101] the difference between these two levels,[102] as well as the precise computational protocol for pK_a[82,103–105] can be found elsewhere. Multiple conformers for both the acid and base species of the photoacids **A–F** (defined in Fig. 1) were taken into account based on the conformer sets that were already determined during the previous study in DMSO.[62] Since the geometries used for COSMO-RS are optimized with COSMO for $\varepsilon_r = \infty$, *i.e.*, they are independent of the solvent, no additional changes were needed. For pK_a in acetone, the parameters for COSMO-RS were taken from ref. 82. Excited-state pK_a^* values are then obtained by adding the ΔpK_a from eqn (1) to the COSMO-RS ground-state pK_a. All calculations refer to a temperature of 298.15 K (25 °C).

3. Results and discussion

3.1 Theoretical spectroscopy in acetone with implicit solvation

3.1.1 Reassessing the method performance for photoacid B. First, the performance of the methods was validated, including the implicit solvent model COSMO, but this time with a focus on photoacid **B** in acetone, as the center of the time-resolved experiments. The vertical (de-)excitation energies obtained with different combinations of methods for the geometry and for the electronic excitations are plotted in Fig. S1 and tabulated in Table S1 (ESI†).

For the protonated form, referred to as acid, the implicit solvent model COSMO introduces a bathochromic (*i.e.*, solvatochromic

 This journal is © the Owner Societies 2023

red) shift between the gas-phase (without COSMO) and solution-phase (with COSMO) excitation energies of ~150 meV at all geometries. Best agreement between the calculated and the experimental results is found for the COSMO-CC2//COSMO-CC2 level in absorption and COSMO-CC2//COSMO-ADC(2) in emission, differing only by 14 meV and 45 meV from the experiment, respectively. For the deprotonated form, referred to as base, implicit solvent effects as described by COSMO again cause a bathochromic shift of ~100 meV for CC2 and <100 meV for ADC(2). Note that best agreement between the calculations and experiments is found in case of the base for absorption again with COSMO-CC2//COSMO-CC2 (differing by 6 meV).

Regarding the reliability of the selected methods, the results for photoacid **B** in acetone are very similar to the previous results for photoacid **F** in DMSO.[62] The absorption energies at the COSMO-CC2//COSMO-CC2 level are in excellent quantitative agreement with the experimental results, whereas the emission energies at the COSMO-CC2//COSMO-ADC(2) level underestimate them by 0.1–0.2 eV. Except for the large deviation for the acid emission energy that is further analyzed later (*vide infra*), these results fall within the typical accuracy of ADC(2) and CC2 that has been observed in benchmarking studies.[106,107]

Since in solution we are restricted to COSMO-ADC(2) geometries because COSMO-CC2 gradients are not available, we use for consistency also the corresponding COSMO-MP2 geometries in the ground state to maintain a consistent description of both electronic states. This seems justified as the corresponding COSMO-CC2//COSMO-MP2 absorption energies likewise only differ slightly (50–70 meV) from the experiments. However, even independent of the method for the geometry, the use of COSMO-CC2 for the excitation energies clearly gives better results. Therefore, COSMO-CC2 excitation energies at COSMO-MP2 (S_0) or COSMO-ADC(2) (S_1) geometries are the default levels in this work.

For photoacid **B**, CC2 still yields slightly smaller excitation energies, which means here better agreement with experiment. Particularly for the absorption of the acid, a monotonous decrease from the MP2, over the COSMO-MP2 and CC2, toward the COSMO-CC2 geometry is observed, independent of the method for the excitation energy. Besides, implicit solvation has a significant effect on the excitation energies, manifesting in the pronounced bathochromic shifts of 100–150 meV, but only a slight to no effect on the geometries (as probed by the excitation energies).

3.1.2 Comparison of photoacids A–F in implicit acetone. In order to compare the ΔpK_a values of the different photoacids in acetone, the UV/Vis absorption and fluorescence emission energies of the compounds **A–F** were calculated in acetone. In accordance with the results from the previous section and results of the previous study in DMSO,[62] the geometries were optimized in the cc-pVDZ basis set using COSMO-MP2 for the ground state and COSMO-ADC(2) for the first excited state. The COSMO-CC2//COSMO-CC2 emission energies were estimated based on the COSMO-CC2//COSMO-ADC(2) results, *i.e.*, COSMO-CC2 energies at the COSMO-ADC(2) excited-state geometries.

3.1.2.1 Agreement between calculated and experimental excitation energies. The calculated UV/Vis absorption and fluorescence emission energies are compared to the experimental results in Fig. 3 and the corresponding numerical values can be found in Table S2 (ESI†). In addition, a statistical analysis of the errors is given in Table 1.

The results show that for the hydroxypyrene-based photoacids COSMO-CC2 does not only perform overall better than COSMO-ADC(2), but also very well in general based on mean absolute errors (MAEs) or root-mean-square errors (RMSEs) of <100 meV (*i.e.*, better than the reported typical accuracy for excitation energies of organic closed-shell molecules in vacuum).[108] The only case where the COSMO-ADC(2) results happen to be closer to the experimental values are the absorption energies of the acid (Fig. 3(a)). The worst results are found for the COSMO-ADC(2) emission energies of the base (Fig. 3(d)), *e.g.*, MAE of 233 meV and maximum absolute error (maxAE) of 290 meV, which appears the most demanding of these four cases due to multiple reasons. First, computational emission energies typically underestimate the experimental fluorescence energies (*cf.* ME mostly equal MAE for S_1 in Table 1) due to the assumption of a fully equilibrated excited-state geometry, which in the current study is also seen in the results for the emission energies of the acids. Second, ADC(2) has been shown to be a less accurate method for the bases of these photoacids due to missing contributions for a proper description of the electronic ground state (*vide supra*). Third, our calculated (de-)excitation energies refer to vertical transitions, whereas the experimental values denote maximum peak positions in UV/Vis absorption or fluorescence emission spectra.

The rather poor performance of COSMO-ADC(2)//COSMO-MP2 absorption energies in case of the base motivated to re-optimize the ground-state geometries at the COSMO-CC2 level and calculate COSMO-CC2//COSMO-CC2 absorption energies (red bars in Fig. 3(a and b)). For the compounds **A–F**, we find that the COSMO-CC2 excitation energies are at the COSMO-CC2 geometries lower than at the COSMO-MP2 geometries, by *ca.* 50 meV for the acids and 25 meV for the bases, resulting in an increased accuracy (Table 1). Note that the smaller effect for the base compared to the acid is in line with the observations and discussion in Section 3.1.1. As demonstrated by an ME close to zero, COSMO-CC2//COSMO-CC2 reveals a good error compensation for the base absorption, in contrast to COSMO-CC2//COSMO-MP2 which consistently overestimated the energies.

*3.1.2.2 Tracking the error for the outlier—photoacid **E**.* Only maxAE (photoacid **E**) has further increased owing to an underestimation of the experimental value already at the COSMO-MP2 geometry that further amplifies for the COSMO-CC2 geometry due to additional stabilization. An important difference between **E** and the other compounds are the additional OH groups in the side chains of the sulfonic acid amide moieties, which offer additional hydrogen-bonding sites.

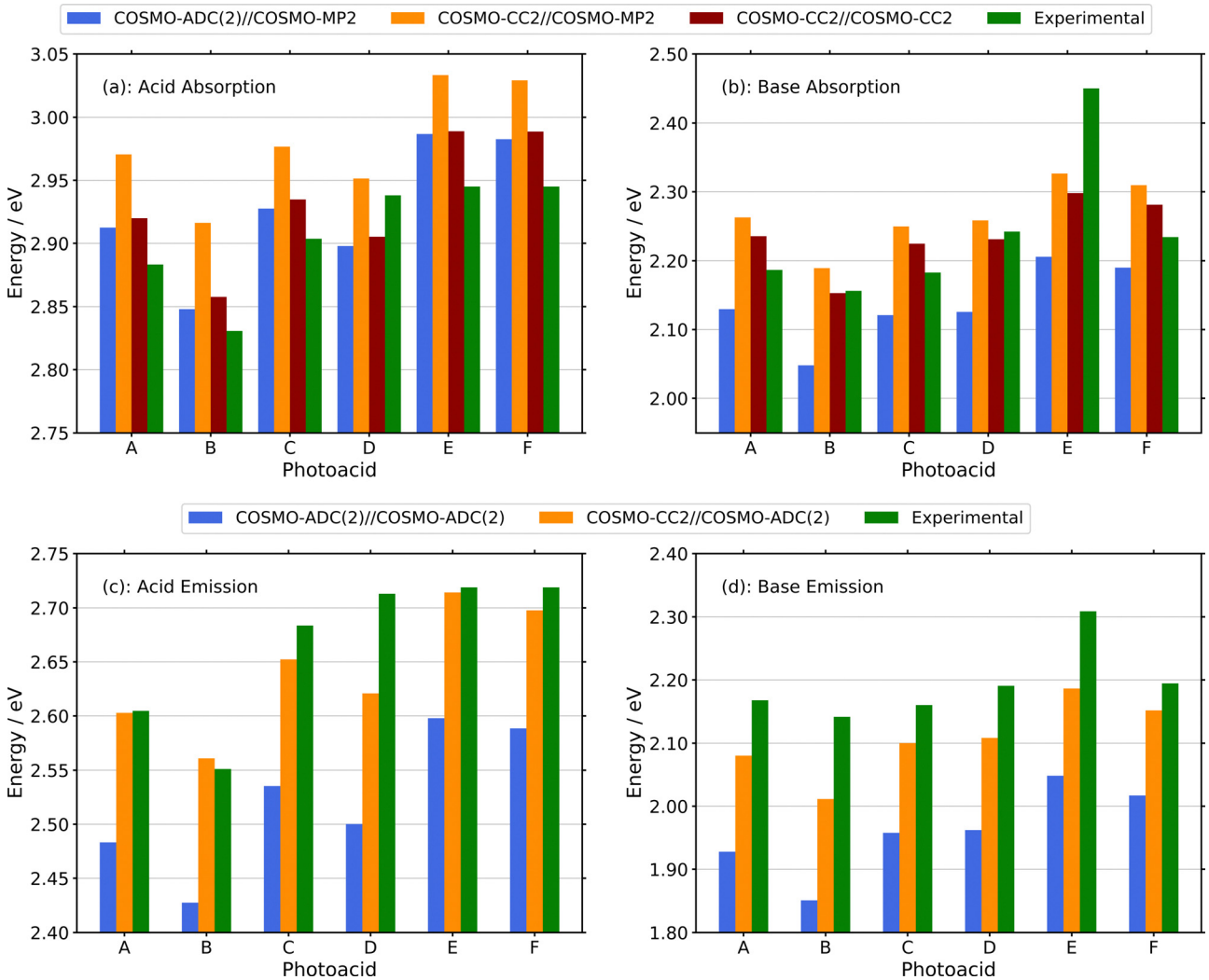


Fig. 3 Theoretical spectroscopy of Jung's photoacids in acetone. Comparison of calculated vertical transition and experimental band maxima energies in eV for UV/Vis absorption (top row) and fluorescence emission (bottom row) for the acid (left) and base (right) forms of the six photoacids **A**–**F** in acetone. Experimental values are taken from the original data from ref. 56.

Table 1 Statistical error analysis of the UV/Vis absorption and fluorescence emission energies of the acid (ROH) and base (RO^-) species of photoacids **A**–**F** in acetone. Mean error (ME), mean absolute error (MAE), maximum absolute error (maxAE), and root-mean-square error (RMSE) based on the calculated COSMO-ADC(2) and COSMO-CC2 vertical transition energies and experimental band maxima (from ref. 56) as shown in Fig. 3. An asterisk is used to differentiate absorption (ROH, RO^-) from emission (ROH*, RO^-*) energies. Values are given in meV

Species	Level	ME	MAE	maxAE	RMSE
ROH	COSMO-ADC(2)//COSMO-MP2	18	32	42 (E)	33
	COSMO-CC2//COSMO-MP2	72	72	88 (E)	77
	COSMO-CC2//COSMO-CC2	25	36	44 (E)	36
ROH*	COSMO-ADC(2)//COSMO-ADC(2)	−143	143	213 (D)	147
	COSMO-CC2//COSMO-ADC(2)	−24	27	92 (D)	41
RO^-	COSMO-ADC(2)//COSMO-MP2	−105	105	244 (E)	125
	COSMO-CC2//COSMO-MP2	24	65	124 (E)	74
	COSMO-CC2//COSMO-CC2	−5	51	152 (E)	70
RO^-*	COSMO-ADC(2)//COSMO-ADC(2)	−233	233	290 (B)	236
	COSMO-CC2//COSMO-ADC(2)	−87	87	130 (B)	93

It turned out that compound **E** is not flexible enough to allow for intramolecular hydrogen bonding (HB), see Fig. 4 and Table 2. Next, self-association, *i.e.*, intermolecular hydrogen bonding between the photoacid OH group at the pyrene moiety of one molecule and an OH group in the side chain of another molecule was conjectured as the cause. To test this, the second photoacid molecule was represented by methanol (MeOH) to decrease the computational costs of the model system (see Fig. 4(h)).

The results for photoacid **E** in Table 2 reveal a strong effect of intermolecular HB donation on RO^- and RO^-*, consisting in blue shifts of ∼60 meV and ∼40 meV, respectively. These shifts reduce the errors from ∼120 meV to only 60–70 meV. Moreover, the results for RO^- and RO^-* both continue to underestimate the experimental value, which is in agreement with the explicit solvent effect of water on the RO^-/RO^-* properties of photoacid **B** in water (see Section 3.2.3.2, Table 7). Since only one HB donor was considered, but each

 This journal is © the Owner Societies 2023

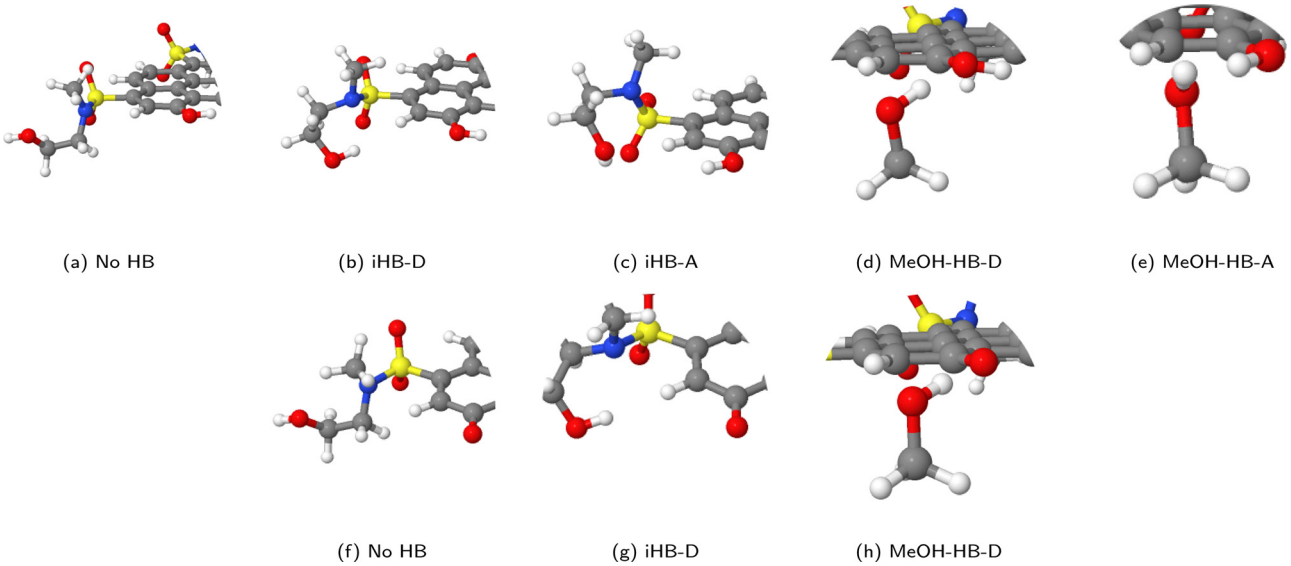


Fig. 4 Intra and intermolecular hydrogen-bonding interactions for photoacid **E**. Magnified acid (top) and base (bottom) structures without HB (No HB), for intramolecular HB (iHB) with the side-chain OH either acting as HB donor (D) or acceptor (A), and for intermolecular HB modeled by an interaction with MeOH acting as HB-D or HB-A. Only HB donation is relevant for the base. All structures have been optimized at the COSMO-MP2/cc-pVDZ level.

Table 2 Shifts induced for photoacid **E** by hydrogen bonding. Comparison of calculated UV/Vis absorption and fluorescence emission energies (*) in eV of the acid (ROH) and base (RO^-) species for different intra and inter-molecular interactions: no interactions (No HB), intramolecular hydrogen bonding (iHB), and intermolecular hydrogen bonding due to self-association (MeOH). The HB role of the side-chain or methanol OH is labeled with D (donor) and A (acceptor). The experimental results are taken from ref. 56

		iHB		MeOH		
Species	No HB	HB-D	HB-A	HB-D	HB-A	Exptl.
ROH	3.033	3.023	3.028	3.068	2.967	2.945
ROH*	2.714	n.a.	n.a.	2.737	2.649	2.719
RO^-	2.326	2.322	—	2.383	—	2.450
RO^-*	2.186	n.a.	—	2.224	—	2.309

molecule of photoacid **E** has one OH group in each of the three substituents, additional blue shifts that would further compensate for that are anticipated.

For the acid, we studied the role of the aliphatic alcohol group modeled by MeOH both as HB donor (Fig. 4(d)) and HB acceptor (Fig. 4(e)). The aromatic OH group is only a weak HB acceptor, but a strong HB donor. For example, phenol—as a model for the pyrenol core of photoacid **E**—has Kamlet–Taft parameters of α = 1.65 (HB donation) and β = 0.30 (HB acceptance), whereas ethanol—as a model for the side-chain OH group—has parameters α = 0.83 and β = 0.77.[109] Consequently, configurations with the aromatic OH group as the HB donor and the aliphatic side-chain OH as the acceptor should be more stable and hence occur more frequently compared to the reverse scenario. For the acid of **E**, the excitation energy is red shifted by ~70 meV by a HB with MeOH as HB acceptor. In contrast, HB donation by MeOH leads to a blue shift by 35 meV. For ROH*, *i.e.*, for emission energies, similar red (65 meV) and blue (23 meV) shifts are found for MeOH acting as a HB acceptor or donor, respectively.

The results for this model (Table 2) overall appear convincing that such intermolecular HB interactions between two or more photoacid molecules are the cause for the deviations of photoacid **E** observed in the results for the set of photoacids **A**–**F** (Fig. 3). Interestingly, no such distinct outlier character for photoacid **E** was found in the previous study in DMSO. This observation is attributed to the higher HB-acceptor strength of DMSO (as also discussed in Section 3.2.2.1) which binds the side-chain OH groups more strongly and hence makes them less available for photoacid–photoacid interactions. This is also in line with the general description of DMSO as an HB breaker in the literature.[110–112]

3.1.2.3 Discussion of acidity increase upon excitation. Through the computational or experimental first electronic excitation energies (*cf.* Fig. 3), the ΔpK_a values, *i.e.*, the change in pK_a upon excitation can be computed based on the Förster cycle (eqn (1)). The corresponding results for COSMO-CC2 have been collected in Table 3 and those for COSMO-ADC(2) can be found in Table S3 (ESI†). Since the better performance of COSMO-CC2 over COSMO-ADC(2), as observed before, is also reflected in the ΔpK_a values of Table 3, we only focus on the COSMO-CC2 results in the following discussion.

That having said, the main focus is set—for brevity—to the ΔpK_a values that are averaged over absorption and emission energies. These are generally in very good agreement with the experimental data, differing by less than one ΔpK_a unit on average. The deviation is slightly larger for photoacids **A** (0.8) and **B** (1.6) and largest for **E** (2.8), with large deviations (~2) for the emission contributions as the main error source. Note that

Table 3 Differences in the photo-induced acidity increase as quantified by ΔpK_a between the photoacids **A**–**F** in the solvent acetone. ΔpK_a based on the Förster cycle (*cf.* eqn (1)) using either absorption, emission, or averaged excitation energies calculated with COSMO-CC2 at the COSMO-MP2 (S_0) and COSMO-ADC(2) (S_1) geometries (taken from Table S2, ESI) and the experimental band maxima (taken from ref. 56)

		Photoacids					
	Level	**A**	**B**	**C**	**D**	**E**	**F**
Absorption	COSMO-CC2	−12.0	−12.3	−12.3	−11.7	−11.9	−12.2
	Experimental	−11.8	−11.4	−12.2	−11.8	−8.4	−12.0
Emission	COSMO-CC2	−8.8	−9.3	−9.3	−8.7	−8.9	−9.2
	Experimental	−7.4	−6.9	−8.9	−8.8	−6.9	−8.9
Averaged	COSMO-CC2	−10.4	−10.8	−10.8	−10.2	−10.4	−10.7
	Experimental	−9.6	−9.2	−10.5	−10.3	−7.6	−10.4

the calculated values always overestimate ΔpK_a in magnitude, with the only exception of photoacid **D**.

In comparison to the previous results in DMSO (*cf.* ref. 62), the calculated averaged COSMO-CC2 ΔpK_a values show a tendency to further decrease (*i.e.*, increase in magnitude) in the less polar solvent acetone. This phenomenon was already observed before when comparing DMSO to water and can be explained based on the different stabilizing effect of the solvent polarity on the four different species (ROH, ROH*, RO^-, RO^-*) involved in the Förster cycle. In the following, photoacid **E** is excluded since its calculated ΔpK_a are based on the results in Fig. 3, which revealed to be outliers (*vide supra*). Although the averaged computed ΔpK_a that is (additionally) averaged over the five remaining photoacids **A**–**D** and **F** only differs slightly, *i.e.*, −10.50 in DMSO *vs.* −10.58 in acetone, the same trend is already reflected in the experimental data. Unfortunately, a direct comparison of averaged experimental ΔpK_a values is prevented by missing experimental data on ROH* emission for **A** and **B** in DMSO. However, on average, the experimental ΔpK_a based on absorption in acetone (−11.84) compares to a value of −10.74 in DMSO. Similarly, this trend is also found in the ΔpK_a based on experimental emission energies which, averaged over compounds **C**, **D**, and **F**, yields values of −8.38 in acetone and −6.38 in DMSO.

In general, the agreement between the experimental and calculated results is overall better for acetone than for DMSO, in line with the weaker, specific solute–solvent interactions in the less HB-accepting (β) solvent acetone. The large deviations observed for compound **E**, when describing an isolated molecule in the solvent cavity, are most probably due to intermolecular interactions between two photoacid molecules (*vide supra*). For the photoacid–methanol complex as a model system, the following ΔpK_a values are obtained instead: −9.9 (absorption), −7.2 (emission), and −8.5 (averaged). These results demonstrate a significantly improved agreement with the experimental values by reducing the errors to only 1.5, 0.3, and 0.9 for absorption, emission, and on average, respectively. Compared to the COSMO-CC2 results without hydrogen bonding, the ΔpK_a in both absorption and emission have changed by roughly two pK_a units, but slightly stronger in absorption.

3.1.2.4 Discussion of ground and excited-state acidities. As can be seen in Table 4, the pK_a at the two levels of theory (BP-TZVP and BP-TZVPD-FINE) are generally quite similar and, more importantly, share common characteristic features. For example, compound **B** is predicted to be the strongest ground-state acid at both levels and the same trends between compounds **A**–**D** are found. The largest deviations between the two levels are found for photoacids **D** (1.3) and **E** (1.2), which causes the overall trends for **A**–**F** to differ between these levels. **D** is the weakest at the BP-TZVP level, while it is **E** for BP-TZVPD-FINE. These general trends in the pK_a values are governed by the electronic effect of the substituents. Photoacids **A** and **B** are the stronger acids owing to their strongly electron-withdrawing trifluoromethyl groups in the ester moieties, while **D**–**F** are the weaker acids due to their less electron-withdrawing amide moieties that are either purely aliphatic (**F**) or carry only distal oxygen-containing functional groups (**D**, **E**). Compound **C** is of medium strength due to its amide substituents—amides are generally less electron-withdrawing compared to esters—that are directly substituted with strongly (inductively) electron-withdrawing methoxy groups.

The resulting pK_a^*, *i.e.*, excited-state pK_a values are also shown in Table 4. Since the acidity increase (ΔpK_a) was found to be very similar for the compounds **A**–**F**, the relative order in pK_a^* is mainly determined by the order in pK_a. As a result, photoacid **B** is predicted to be the strongest excited-state acid with a pK_a^* (on average) around 3.6, followed by **A** (5.1), **C** (7.8), **E** (9.6) and **F** (9.4), leading to **D** (10.1) as the weakest acid in the excited state. These results are in line with those in the solvent DMSO. However, two main differences compared to DMSO should be noted. First, the pK_a^* values cover a larger range in acetone (6.5) compared to DMSO (4.6) or water (3.1), which is due to the reduced pK_a windows in these solvents. Second, all pK_a^* values are strongly positive which indicates a much lower tendency for ESPT. This is due to the largely positive ground-state pK_a values, as a consequence of the low bulk basicity of the solvent acetone. Thus all compounds **A**–**F** are expected to be weaker acids than the protonated solvent, which means that ESPT is thermodynamically unfavorable ($\Delta G_{diss} > 0$). Still, photoacid **B** is closest to this threshold value, thus suggesting the largest ESPT yield in acetone, which matches

Table 4 Comparison of calculated ground-state and excited-state acidities of the photoacids **A**–**F** in the solvent acetone. pK_a values using COSMO-RS at the BP-TZVP (and BP-TZVPD-FINE) level, ΔpK_a based on the Förster cycle using the averaged excitation energies at the COSMO-CC2 level (taken from Table 3), and pK_a^* based on these input quantities according to eqn (1)

	Photoacids					
	A	**B**	**C**	**D**	**E**	**F**
pK_a	15.6 (15.4)	14.2 (14.7)	18.6 (18.5)	20.9 (19.6)	19.4 (20.6)	19.9 (20.3)
ΔpK_a	−10.4	−10.8	−10.8	−10.2	−10.4	−10.7
pK_a^*	5.2 (5.0)	3.4 (3.9)	7.8 (7.7)	10.7 (9.4)	9.0 (10.2)	9.2 (9.6)

This journal is © the Owner Societies 2023

the experimental finding that ESPT to solvent is observed only for this compound.[55]

3.2 Beyond implicit solvation

Apart from **E** where self-association seems to effect the experimental values, the results for photoacid **B** exhibit one of the largest deviations between the calculated and the experimental ΔpK_a values (*cf.* Table 3), especially regarding the emission energies. Furthermore, the experimental results have shown that specific molecular interactions between the photoacid **B** and the solvent or other proton acceptors become relevant in acetone solution.[60] This motivated us to include explicit solvent molecules in the first solvation shell and to study their effect on the electronic excitation energies of this photoacid.

It is important to note that the way of including explicit solvent that is followed here is purely based on chemical intuition and does not constitute an approach that aims at systematically improving the calculated results up to perfect agreement with the experiments, which would, *e.g.*, require MD simulations to obtain representative solvation structures. Rather, micro-solvated structures for hydrogen-bonding configurations that appear most relevant based on the Kamlet–Taft parameters are considered (*vide infra*). In particular, a strict comparison of the absolute excitation energies with the experimental results is thus not meaningful, mainly because of two reasons: (i) an uncertainty due to the (larger) intrinsic errors compared to the observed (smaller) solvatochromic shifts induced by explicit solvent, and (ii) a possible overestimation of the solvatochromic shifts due to the neglect of solvent fluctuation causing smaller HB distances at the equilibrium structures compared to the thermodynamic ensemble average. Therefore, the focus will be instead set to the differential effect (of explicit solvent) between the acid and base, *i.e.*, the effect on ΔpK_a^*, since large parts of these two errors are anticipated to cancel therein.

3.2.1 Kamlet–Taft considerations. To compare the effect of explicit solvation on the spectral properties of the four species (ROH, ROH*, RO^-, and RO^-*) in different environments, the solvents acetone, DMSO, and water were selected. This selection is chosen for comparison with experiments since all three solvents were already part of experimental studies.[55,56]

Per definition, acetone and DMSO have as aprotic solvents no or only a very small tendency to act as hydrogen-bond (HB) donors (HB-Ds) as quantified, *e.g.*, by the Kamlet–Taft solvent parameter α (0.08 for acetone and 0.00 for DMSO).[109] They mostly act as HB acceptors (HB-As) as quantified, *e.g.*, by the Kamlet–Taft parameter β (0.48 for acetone and 0.76 for DMSO). In contrast, water—as a dipolar protic solvent—can act as both a strong HB-D ($\alpha = 1.17$) and a moderate HB-A ($\beta = 0.47$). Thus, in this set of solvents, DMSO is the weakest HB-D and strongest HB-A, while water is the strongest HB-D, and water and acetone are the weakest HB-As. For photoacid **B** (referring to phenol as a model), the OH group can either act as a weak HB-A ($\alpha = 0.30$) or strong HB-D ($\beta = 1.65$), whereas the O^- group can only accept hydrogen bonds from other solvent molecules.

Micro-solvated structures were generated by manually adding a given number of explicit solvent molecules according to the target HB configuration to the molecular structure of the implicitly solvated photoacid species and then re-optimizing the full structure embedded in a COSMO cavity. In particular, the S_0 equilibrium geometries, used for the calculation of ROH and RO^- absorption energies, are optimized at the COSMO-MP2/cc-pVDZ level, whereas the S_1 equilibrium structures, used for the calculation of ROH* and RO^-* emission energies, are optimized at the COSMO-ADC(2)/cc-pVDZ level. All excitation energies are typically calculated with COSMO-CC2/aug-cc-pVDZ.

3.2.2 Explicit solvent effects in acetone and DMSO

3.2.2.1 Local solvation in acetone and DMSO. Due to their similarity, the results for the solvents acetone and DMSO are discussed first. One explicit solvent molecule was included to locally solvate the OH or O^- group. Resulting from our considerations regarding the HB characteristics of the different photoacid species as well as the solvents (*vide supra*), we chose the solvent to act as HB-A for ROH/ROH* (Fig. 5(b and c)) and to act as a HB-D for RO^-/RO^-* (Fig. 5(e and f)). Due to the similarity between the S_0 and S_1 equilibrium structures, only those for S_0 are shown in Fig. 5. In Table 5, the excitation energies for these micro-solvated structures in both solvents are compared to those with the purely implicit solvent model COSMO and the experimental reference values.

For both solvents, larger solvatochromic effects—due to the inclusion of explicit solvent—are found for the protonated species ROH and ROH*: red shifts of roughly 80–90 meV in acetone and 110–170 meV in DMSO. In contrast, for RO^- and RO^-*, the shifts fall below 10 meV, which is in agreement with the low HB-D ability of these solvents. Furthermore, the larger shifts for ROH and ROH* in DMSO compared to acetone emphasize the stronger HB acceptance of DMSO.

3.2.2.2 Effect on acidity increase in acetone and DMSO. Using the excitation energies for the micro-solvated structures in acetone and DMSO (Table 5), the Förster-cycle ΔpK_a values *via* eqn (1) were re-calculated, as given in Table 6. In accordance with the larger errors associated with the emission energies, the results in Table 6 show that the ΔpK_a improve significantly for both solvents, in absorption as well as emission. For example, we find a change of 1.27 units in the absorption ΔpK_a for acetone, while the fluorescence ΔpK_a changes by 1.43 units, which drastically improves the error from >2 (2.3) to <1 (0.87).

For DMSO, the absorption ΔpK_a strongly improves by roughly 2 units, achieving an excellent agreement with the experiment (residual error <0.1), whereas the fluorescence reveals an even more drastic change of ~ 2.8 units. Unfortunately, no comparison with the experiment is possible due to the missing experimental fluorescence emission energy for ROH* in DMSO. However, the larger changes in both calculated absorption and emission ΔpK_a highlight the larger HB-acceptor ability of DMSO over acetone.

Similar solvatochromic shifts and effects on ΔpK_a are also observed for the photoacids **A** and **F** with explicit acetone or

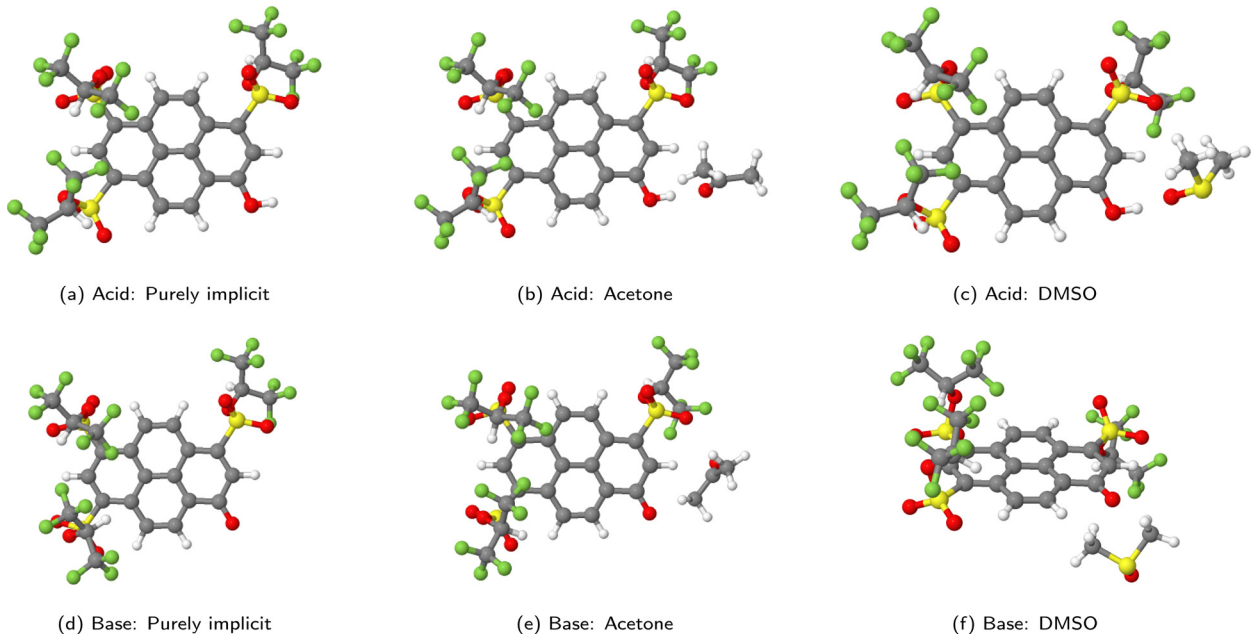


Fig. 5 Implicitly solvated and micro-solvated structures of photoacid **B** in acetone and DMSO. Acid (top) and base (bottom) structures without explicit solvent (purely implicit; left) and with one explicit acetone (middle) or DMSO (right) molecule. All structures have been optimized at the COSMO-MP2/cc-pVDZ level.

Table 5 Solvatochromic shifts due to explicit solvent in the first solvation shell of photoacid **B** in the solvents acetone and DMSO. Comparison of calculated UV/Vis absorption (ROH, RO^-) and fluorescence emission energies (ROH*, RO^-*) in eV of the acid and base species. Results are given for the structures without explicit solvent in purely implicit solution and with one explicit solvent molecule. Experimental results are taken from ref. 55 and 56 for acetone and DMSO, respectively

	Acetone			DMSO		
Species	Impl.	Expl.	Exptl.	Impl.	Expl.	Exptl.
ROH	2.916	2.837	2.831	2.882	2.769	2.761
ROH*	2.573	2.481	2.551	2.539	2.373	—
RO^-	2.191	2.187	2.156	2.155	2.164	2.153
RO^-*	2.027	2.020	2.141	1.995	1.997	2.134

DMSO (see Table S4, ESI†), in line with the findings for photoacid **B**. Therefore, we find some strong indications here that the largest contributions to the error with respect to experiment for the purely implicitly solvated photoacid in acetone and DMSO are missing HB interactions of the solvent with the photoacid OH group, especially the HB donation of ROH*.

3.2.3 Explicit solvent effects in water

3.2.3.1 Local solvation in water—one explicit water molecule. Compared to the aprotic solvents acetone and DMSO, the situation in the protic solvent water is more complicated due to more extensive hydrogen bonding (see Fig. 6). The OH group of the photoacid can only donate one hydrogen bond, but accept up to two. Similarly, the O^- group could in principle accept up to three hydrogen bonds. Therefore, micro-solvated structures with varying numbers of water molecules and with different HB configurations need to be considered. As in Section 3.2.2.1, the explicit solvent was added manually to the structures in implicit solution of the respective solvent and were subsequently re-optimized. The corresponding results for different structures are shown in Table 7. Due to the similarity between the S_0 and S_1 structures, only the former ones are displayed.

Comparing the results in Table 7 for the implicitly solvated species and those including one explicit water molecule (Fig. 6(a, b and f)) demonstrates that the specific hydrogen-bonding role of the solvent matters. When acting as a HB donor, explicit water causes a solvatochromic blue shift for all species: largest for RO^-* (53 meV), slightly smaller for RO^- (43 meV) and ROH* (40 meV), and almost zero for ROH (2 meV). In contrast, when acting as a HB acceptor, red shifts are observed: 91 meV for ROH and 85 meV for ROH*. In comparison with the results for acetone and DMSO (Section 3.2.2), the solvatochromic red shifts follow the order of the solvents in HB-acceptor strength (β): DMSO > acetone $\gtrsim$ water (*cf.* Section 3.2.1 for the β values). Consistent blue shifts due to the solvent acting as the HB donor could only be observed for water since the HB-donating ability of acetone and DMSO are close to zero.

The trends that are observed here indicate that the excitation energies of the base are underestimated much more strongly compared to the acid. It is also physically plausible that for the negatively charged base more hydrogen bonds are relevant than for the acid. Therefore, we considered the addition of additional water molecules to the first solvation shell in the following.

 This journal is © the Owner Societies 2023

Table 6 Effect of explicit solvent on the ΔpK_a of photoacid **B** in acetone and DMSO. Calculated ΔpK_a based on the Förster cycle (*cf.* eqn (1)) using absorption, emission, or averaged energies for implicitly as well as explicitly solvated structures (*cf.* Table 5) in comparison with the experimental ΔpK_a values (*cf.* Table 3) using the data from ref. 55 and 56

	Acetone			DMSO		
	Implicit	Explicit	Experimental	Implicit	Explicit	Experimental
Absorption	−12.26	−10.99	−11.42	−12.29	−10.23	−10.28
Emission	−9.23	−7.80	−6.93	−9.20	−6.36	—
Average	−10.75	−9.40	−9.18	−10.75	−8.30	—

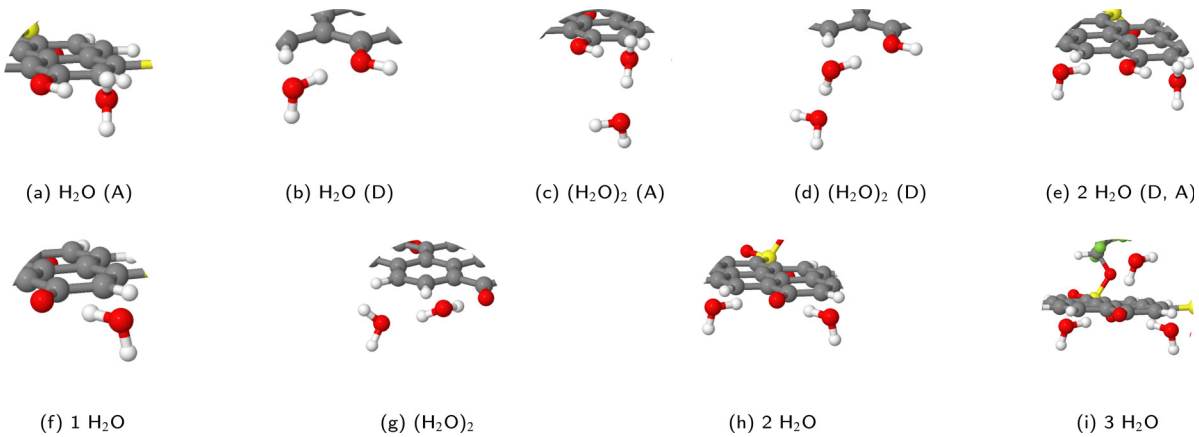


Fig. 6 Micro-solvated structures of photoacid **B** in water for different numbers of explicit solvent molecules. Magnified acid (top) and base (bottom) structures with up to three explicit water molecules, either as HB donors (D) or acceptors (A). Water exclusively acts as HB D for the base. All structures at the COSMO-MP2/cc-pVDZ level.

Table 7 Solvatochromic shifts due to explicit solvent in the first solvation shell of photoacid **B** in the solvent water. Comparison of calculated UV/Vis absorption (ROH, RO^-) and fluorescence emission energies (ROH*, RO^-*) of the acid and base species. Results are given for the structures without explicit solvent in purely implicit water and with up to three explicit water molecules as either HB donor (D) or acceptor (A). Experimental results are taken from ref. 55

	Water								
		1 H_2O		2 H_2O		$(H_2O)_2$		3 H_2O	
Species	Implicit	HB-D	HB-A	HB-D, HB-A	HB-D, HB-D	HB-D	HB-A	HB-D	Experimental
ROH	2.913	2.915	2.822	2.814	—	2.908	2.758	—	3.00
ROH*	2.562	2.602	2.477	2.502	—	2.604	2.435	—	2.53
RO^-	2.202	2.245	—	—	2.268	2.231	—	2.311	2.36
RO^-*	2.032	2.085	—	—	2.112	2.088	—	2.144	2.20

3.2.3.2 Local solvation in water—two (and more) explicit water molecules. Perhaps not the most intuitive but a very simple case of adding two water molecules consists in its dimer, *i.e.*, $(H_2O)_2$ (Fig. 6(c, d and g)) whose effect on the excitation energies is actually very similar to that of a single water molecule. In details, no pronounced effect for HB donation but a red shift of 155 meV for HB acceptance (larger than 1 H_2O) are found for ROH, whereas ROH* reveals a small blue shift of 42 meV (close to 1 H_2O) or a red shift of 127 meV (larger than 1 H_2O). Consequently, the HB donation of the dimer is comparable to that of the monomer, while the HB acceptance is enhanced—in line with a positive polarization of the oxygen of the water accepting the HB from the photoacid due to the HB donation of the second water molecule. In analogy, since only HB donation matters for the anion, blue shifts (very similar to 1 H_2O) of 29 meV and 56 meV are observed for RO^- and RO^-*, respectively.

The photoacid OH (O^-) group can also form more than one hydrogen bond with the solvent. For two water molecules, the following cases were considered: (i) both acting as HB donors and (ii) one acting as a HB donor and one as a HB acceptor. For the protonated form, scenario (i) was found to be unstable in the calculations (preferring intra-H_2O HB), leaving only (ii) to be considered; while (i) is the relevant case for the deprotonated form. The mixed HB motif (ii) (Fig. 6(e)) yields a red shift of 99 meV for ROH, *i.e.*, slightly larger compared to HB-D for 1 H_2O, and an overall red shift of 60 meV for ROH*

that falls in between the HB-D and HB-A shifts for a single H_2O. This larger similarity in the ROH result to HB-D for 1 H_2O reflects a more dominant effect of HB donation. Similarly, blue shifts of 66 meV (RO^-) and 80 meV (RO^-*) are found for the HB motif (i) (Fig. 6(h)), which are larger than the results for 1 H_2O and make a step in reducing the gap to the experimental value. Finally, the case of micro-solvation with three water molecules as HB donors was studied (Fig. 6(i)) for the RO^- and RO^-* species, mainly motivated by its negative charge. These results reveal even larger blue shifts of 124 meV for RO^- and 112 meV for RO^-*, constituting in an apparent improvement with respect to the experiments.

3.2.3.3 Effect on acidity increase in water. Due to the different possible HB configurations in water, inclusion of explicit solvent effects on ΔpK_a becomes more involved for this solvent. We assumed for all cases that the number of water molecules and types of hydrogen bonds is the same in both electronic states.

For the results purely based on the implicit solvent model COSMO (implicit in Table 8), the deviation from the experimental average ΔpK_a in water is dominated by the error from the emission contribution (>3) rather than the absorption contribution (~ 1.2), yielding an overall error of 2.3 pK_a units. When including one explicit water molecule, the HB interaction with the photoacid as the HB donor and water as the HB acceptor is expected to be most relevant based on the Kamlet–Taft parameters. For this configuration (1 H_2O (HB-A) in Table 8), significant changes of ~ 2.3 units in both the ΔpK_a in absorption and in emission are observed, improving the agreement with the experimental results. In contrast, for the less relevant configuration with water as the HB donor (1 H_2O (HB-D) in Table 8), only a weak effect on ΔpK_a is found, reflecting the much smaller changes in the absolute energies for water as HB-D compared to HB-A (*cf.* Table 7). In fact, the ΔpK_a values with water as a HB donor for ROH and ROH* have larger contributions from the effect on RO^- and RO^-* instead. Thus, even if the (less relevant) HB donation of water occurs, the effect on ΔpK_a is much smaller. Studying the effect of further solvation of the base with up to three water molecules as HB donors, the configuration for the acid with one water molecule (as HB acceptor) is retained in the following. In the progression 1 $H_2O \rightarrow 2\ H_2O \rightarrow 3\ H_2O$ at RO^- and RO^-*, the previous trends in in the evolution of ΔpK_a continue.

The strongest changes—and improvements—in ΔpK_a were observed upon inclusion of the first water molecule, which are dominated by the effect of water as a HB acceptor for both ROH and ROH*, as discussed before. Therefore, the fact that the ΔpK_a in absorption starts to underestimate the experimental value already with one explicit water molecule (as HB acceptor for ROH/ROH*), might refer to an overestimation of the red shifts of ROH and ROH* (with water as a HB acceptor) relative to the blue shifts of RO^- and RO^-* (with water as a HB donor). As pointed out before, such issues concerning solvatochromic shifts are common since the geometry-optimized micro-solvated structures will typically have shorter HB distances compared to the ensemble average. Apparently, this issue is more severe for the acid than the base, possibly due to the charges, *i.e.*, a larger error due to a shorter HB distance in the micro-solvated structures of the non-charged acid compared to the negatively charged base. For comparison, RO^- and RO^-* also experience a systematic step-wise evolution in the absolute energies from 0 H_2O (purely implicit) to 3 H_2O, while remaining underestimations of the experimental results (*cf.* Table 7), which seems a physically correct description.

In summary, this section has demonstrated that the largest contributions to the deviation between the ΔpK_a from calculations in implicit water and the experiments are due to the missing HB interactions of the OH group of the acid species as a HB donor and the O^- group of the corresponding base as a HB acceptor.

3.2.4 Specific photoacid–base interactions in acetone–water mixtures. Lastly, the effect of specific photoacid–co-solvent interactions is studied for acetone–water mixtures, in which acetone and water can compete with each other for the hydrogen-bonding sites of the photoacid.

3.2.4.1 Spectral evolution in bulk acetone–water mixtures. The experimental UV/Vis absorption spectra of the protonated form of photoacid **B** revealed a noticeable peak progression with increasing water content in acetone–water mixtures.[60] Moreover, it was also already inferred from the experimental data that a photoacid–water complex with the stoichiometry [ROH·H_2O] is formed under these conditions. To test if such as peak progression could be simply caused by a bulk electrostatic effect of changes in the solvent composition, we applied the calculation of electronic excitation energies with the continuum solvation model COSMO to these solvent mixtures. Due to the large similarity between the refractive indices of water (1.333) and acetone (1.359), only the effect through the relative dielectric constant (ε_r) was considered, which is known to vary linearly with the weight fraction of water in acetone.[113] The UV/Vis absorption energies for the first transition calculated at the fixed COSMO-CC2/cc-pVDZ geometry optimized in acetone but using the ε_r value of the respective acetone-water mixtures for the COSMO-CC2/aug-cc-pVDZ excitation energy calculations are given in Table 9.

Table 8 Effect of explicit solvent on the ΔpK_a of photoacid **B** in water. Calculated ΔpK_a based on the Förster cycle (eqn (1)) using absorption, emission, or averaged energies for implicitly as well as explicitly solvated structures in comparison with the experimental ΔpK_a values using the data from ref. 55, (*cf.* Table 7). Whereas the contribution for RO^- and RO^-* refers to the respective number of water molecules exclusively acting as HB donors, just one water molecule as either donor (HB-D) or acceptor (HB-A) is considered for ROH and ROH*

	Water					
		1 H_2O				
	Implicit	HB-D	HB-A	2 H_2O	3 H_2O	Explt.
Absorption	−12.02	−11.33	−9.75	−9.36	−8.64	−10.78
Emission	−8.96	−8.74	−6.63	−6.17	−5.63	−5.61
Average	−10.49	−10.04	−8.19	−7.77	−7.14	−8.20

This journal is © the Owner Societies 2023

Table 9 Spectral evolution in acetone–water mixtures. Comparison of the calculated (vertical) UV/Vis absorption wavelength of the acid species (ROH) of photoacid **B** in different acetone–water mixtures as modeled by variation of the relative dielectric constant ε_r. Each solvent mixture is characterized by its water content as expressed by the concentration $c(H_2O)$, molar fraction $x(H_2O)$, and weight fraction $w(H_2O)$, together with the associated ε_r value based on a linear interpolation (R^2 = 0.999) of the data from ref. 113. For further reference, the results in bulk water (ε = 78.30) are also included. Experimental values are taken from ref. 60

				λ/nm	
$c(H_2O)$/mol L^{-1}	$x(H_2O)$/%	$w(H_2O)$/%	ε_r	Calc.	Exptl.
0.0	0.0	0.0	20.56	433.89	436
0.8	5.8	1.9	21.64	433.94	438
1.6	11.0	3.7	22.68	434.00	439
2.4	15.6	5.4	23.68	434.05	440
3.1	19.7	7.1	24.65	434.09	440
4.1	24.7	9.2	25.89	434.15	441
(55.6)	100	100	78.30	434.88	414

A comparison of the calculated results in neat implicit acetone (ε_r= 20.56) and water (ε_r = 78.30) demonstrate that a very small ε_r-related red shift between the two solvents is observed, from a wavelength of *ca.* 434 nm in acetone to a wavelength of *ca.* 435 nm in water. Since the experimental absorption maximum in water (414 nm) is actually blue-shifted relative to that in acetone (436 nm), the experimentally observed spectral changes cannot be a purely electrostatic bulk effect. Rather, these changes appear to be due to specific intermolecular interactions. This observation is in line with the calculations. While the solvent composition changes dramatically on a molecular level within a concentration range of 0.0 to 4.1 mol L^{-1}, reaching a final mole fraction of *ca.* 25%, the changes in ε_r are much more subtle, increasing only from 20.56 to 25.89 due to the more weakly pronounced linear dependence in the volume fraction. The ROH absorption peak undergoes indeed a red shift from 436 nm to 441 nm in the experiments, but this is not equally reflected in the calculations that yield a more or less constant value of *ca.* 434 nm, despite a correct and yet very weak shift to the red.

3.2.4.2 Specific photoacid–base interactions. To study the effect of water molecules as competing HB partners in acetone, we re-calculated the UV/Vis absorption of the hydrogen-bonded complexes of the acid species. Absorption energies were calculated using COSMO-CC2/aug-cc-pVDZ at re-optimized COSMO-MP2/cc-pVDZ geometries in implicit acetone. The corresponding results are compiled in Table S5 (ESI†).

The result with one explicit acetone molecule (437 nm) is in almost perfect agreement with the experimental value (436 nm, Table 9). When exchanging the acetone by a water molecule as a HB acceptor in the [ROH·S] complex (where S represents the solvent), the associated solvatochromic red shift increases (reaching 445 nm), matching the experimental peak progression in acetone–water mixtures upon addition of water (Table 9). In a first approximation, the HB interaction energy is for water (as a HB acceptor) ~18 kJ mol^{-1} weaker in energy compared to acetone, in line with the HB-acceptor strengths.

Besides, water can also act as a HB donor. Despite of being the weaker interaction (disfavored by ~26 kJ mol^{-1} compared to HB acceptor), this configuration leads to a blue shift (toward 425 nm). Interestingly, the large experimental blue shift of the ROH absorption maximum in water (414 nm) with respect to the COSMO prediction in implicit water (435 nm) (*cf.* Table 9)—in view of the good agreement in acetone instead (434 nm calc. *vs.* 436 nm exptl.)—implies that the HB donation will effectively take over at some critical water content. This means that there should be a two-step progression upon addition of water, *i.e.*, first, at low concentrations, the observed red shift and second, at higher concentrations, a counteracting blue shift. Interestingly, this was not yet experimentally observed due to the restriction to a maximum of *ca.* 4 M (25%) water. Still, the calculations lead us to infer that the experimental peak progression is indeed caused by the formation of photoacid–water complexes *via* a displacement of acetone molecules in the first coordination shell.

4. Conclusions

This work has extended the previous approach for the theoretical spectroscopy of Jung's photoacids using the implicit solvent model COSMO in combination with the wavefunction-based methods ADC(2) and CC2 to the solvent acetone. Revalidation of the selected methods demonstrated that COSMO-CC2/aug-cc-pVDZ excitation energies still achieve a good agreement with the experimental UV/Vis absorption and fluorescence emission energies in acetone, in fact even better in direct comparison with DMSO. However, the further improvement with COSMO-CC2 compared to COSMO-MP2 geometries motivated for a switch to COSMO-CC2/cc-pVDZ geometries, which is currently restricted in TURBOMOLE to the ground state due to the missing implementation of COSMO-CC2 excited-state gradients.

Regarding an absolute agreement between the calculated and experimental absorption and emission energies, COSMO-CC2 yields mean absolute errors and root-mean-square errors smaller than 0.1 eV for photoacids **A–F** in acetone. The agreement is generally slightly better for the acid compared to the base species and for absorption compared to emission. With COSMO-CC2 ground-state geometries, even an MAE of less than 0.05 eV is obtained. In most cases, photoacid **E** was found to be the largest outlier, which could be traced back to intermolecular hydrogen-bonding interactions between the photoacidic OH group (or O^- after deprotonation) and the additional OH groups in the side chains, which in the calculations have been modeled by a photoacid–methanol complex. Photoacid **E** had not been specifically identified as an outlier in the previous study in DMSO, in line with higher HB donation of the latter leading to stronger interactions with the photoacids and preventing intermolecular HB among them.

The calculations using the implicit solvent model COSMO in combination with CC2 predict averaged (over absorption and emission) ΔpK_a values in the range of −11 to −10 for all the photoacids studied here, in good agreement with the experimental results. Moreover, the change in ΔpK_a when comparing the two solvents DMSO and acetone fits to the trend regarding the solvent polarity that was already observed and rationalized in our previous studies. Similar to the previous results in DMSO, the order in pK_a^* is mainly determined by the order in pK_a since ΔpK_a is virtually identical for all of these photoacids. However, due to their much weaker ground-state acidities in acetone, these photoacids have a much lesser tendency to protonate the solvent. Only photoacids **A** and **B** are expected to perform an efficient ESPT in acetone.

Another focus was set to going beyond implicit solvation and accounting for explicit solvent effects by comparing the solvents acetone, DMSO, and water. For this, instead of performing MD simulations, explicit solvent molecules in the first solvation shell of the photoacids were incorporated for the most relevant HB configurations, as judged based on the Kamlet–Taft parameters. By going beyond implicit solvation, it could be shown that the largest missing contributions to ΔpK_a are due to HB interactions with the solvent. For the aprotic solvents acetone and DMSO, one explicit solvent molecule appeared sufficient, in agreement with the simplified HB interactions in these solvents. These solvents can only efficiently act as HB acceptors for the OH group of the acid species, leading to a bathochromic shift in the absorption and emission, but barely interact with the base species due to the lack of HB donation. In contrast, the situation was much more difficult in the protic solvent water, which can act as both a HB donor and acceptor. The additional HB interaction with the solvent as HB donor and the base species as HB acceptor was verified as another relevant interaction.

Finally, water and acetone were compared as complexation partners for photoacid **B** in acetoneous solution. The calculations provided supporting evidence that the experimentally observed spectral evolution in acetone–water mixtures is due to a specific molecular interaction, rather than a bulk effect. Interestingly, the experimental absorption band of the acid species is blue-shifted in water relative to acetone, although the initial peak progression upon addition of water consists in a red shift, indicating that water at very low concentrations is dominantly acting as HB acceptor, but that at larger concentrations the effect HB donation dominates the solvent shift. This interesting observation provides a motivation to study acetone–water mixtures of the full range of the water content to further investigate these changes.

In order to further improve the agreement with the experiments, a more accurate description of the solvation is anticipated most relevant, which will inevitably require MD simulations with explicit solvent for sampling the configuration space and finding representative structures. For best comparison with the experiments, both UV/Vis absorption and fluorescence emission energies are needed as usually an average of these two quantities is used to determine ΔpK_a experimentally. Apart from the rather large size of these photoacids, this need for sampling the first electronically excited state appears most demanding.

Author contributions

Niklas Sülzner: conceptualization, methodology, validation, investigation, formal analysis, visualization, data curation, writing – original draft. Christof Hättig: conceptualization, supervision, project administration, resources, funding acquisition, writing – review & editing.

Conflicts of interest

There are no conflicts to declare.

Acknowledgements

We acknowledge financial support by the Deutsche Forschungsgemeinschaft through project Ha 2588/10-1. Funded by the Deutsche Forschungsgemeinschaft (DFG, German Research Foundation) under Germany's Excellence Strategy–EXC 2033–390677874–RESOLV.

Notes and references

1 P.-T. Chou and K. M. Solntsev, *J. Phys. Chem. B*, 2015, **119**, 2089.
2 H. Kagel, M. Frohme and J. Glökler, *J. Cell. Biotechnol.*, 2018, **4**, 23–30.
3 S. Hammes-Schiffer, *J. Phys. Chem. B*, 2021, **125**, 3725–3726.
4 P. Leiderman, D. Huppert, S. J. Remington, L. M. Tolbert and K. M. Solntsev, *Chem. Phys. Lett.*, 2008, **455**, 303–306.
5 C. Chen, L. Zhu, M. S. Baranov, L. Tang, N. S. Baleeva, A. Y. Smirnov, I. V. Yampolsky, K. M. Solntsev and C. Fang, *J. Phys. Chem. B*, 2019, **123**, 3804–3821.
6 Y. Erez and D. Huppert, *J. Phys. Chem. A*, 2010, **114**, 8075–8082.
7 J. Kuchlyan, D. Banik, N. Kundu, S. Ghosh, C. Banerjee and N. Sarkar, *J. Phys. Chem. B*, 2014, **118**, 3401–3408.
8 V. O. Silva, A. A. Freitas, A. L. Maçanita and F. H. Quina, *J. Phys. Org. Chem.*, 2016, **29**, 594–599.
9 F. H. Quina, P. F. Moreira, C. Vautier-Giongo, D. Rettori, R. F. Rodrigues, A. A. Freitas, P. F. Silva and A. L. Maçanita, *Pure Appl. Chem.*, 2009, **81**, 1687–1694.
10 D. Pines and E. Pines, *Hydrogen-Transfer Reactions*, John Wiley & Sons, Ltd, 2006, pp. 377–415.
11 *Proton-Transfer Reactions*, ed. E. Caldin and V. Gold, Springer US, Boston, MA, 1975.
12 J. Reijenga, A. van Hoof, A. van Loon and B. Teunissen, *Anal. Chem. Insights*, 2013, **8**, ACI.S12304.
13 B. Pathare, V. Tambe and V. Patil, *Int. J. Pharm. Pharm. Sci.*, 2014, **6**, 26–34.

 This journal is © the Owner Societies 2023

14 K. S. Alongi and G. C. Shields, in *Annual Reports in Computational Chemistry*, Elsevier, 2010, vol. 6, pp. 113–138.
15 P. G. Seybold and G. C. Shields, *Wiley Interdiscip. Rev.: Comput. Mol. Sci.*, 2015, **5**, 290–297.
16 J. F. Ireland and P. A. H. Wyatt, in *Advances in Physical Organic Chemistry*, Academic Press, 1976, vol. 12, pp. 131–221.
17 N. Agmon, *J. Phys. Chem. A*, 2005, **109**, 13–35.
18 N. M. Trieff and B. R. Sundheim, *J. Phys. Chem.*, 1965, **69**, 2044–2059.
19 L. G. Arnaut and S. J. Formosínho, *J. Photochem. Photobiol., A*, 1993, **75**, 1–20.
20 M. Rini, B.-Z. Magnes, E. Pines and E. T. J. Nibbering, *Science*, 2003, **301**, 349–352.
21 C. Hoberg, J. Talbot, J. Shee, T. Ockelmann, D. DasMahanta, F. Novelli, M. Head-Gordon and M. Havenith, *Chem. Sci.*, 2023, DOI: **10.1039/D2SC07126F**.
22 Y. Wang, W. Liu, L. Tang, B. Oscar, F. Han and C. Fang, *J. Phys. Chem. A*, 2013, **117**, 6024–6042.
23 J. Saway, Z. M. Salem and J. J. Badillo, *Synthesis*, 2021, 489–497.
24 O. S. Wolfbeis and E. Koller, *Anal. Biochem.*, 1983, **129**, 365–370.
25 Z. Zhujun and W. R. Seitz, *Anal. Chim. Acta*, 1984, **160**, 47–55.
26 J. A. Menges, A. Clasen, M. Jourdain, J. Beckmann, C. Hoffmann, J. König and G. Jung, *Langmuir*, 2019, **35**, 2506–2516.
27 J. A. Menges, A. Grandjean, A. Clasen and G. Jung, *ChemCatChem*, 2020, **12**, 2630–2637.
28 R. Simkovitch, D. Pines, N. Agmon, E. Pines and D. Huppert, *J. Phys. Chem. B*, 2016, **120**, 12615–12632.
29 R. Simkovitch, G. G. Rozenman and D. Huppert, *J. Photochem. Photobiol., A*, 2017, **344**, 15–27.
30 L. Genosar, B. Cohen and D. Huppert, *J. Phys. Chem. A*, 2000, **104**, 6689–6698.
31 A. A. Awasthi and P. K. Singh, *Chem. Phys. Chem.*, 2018, **19**, 198–207.
32 O. Gajst, L. Pinto da Silva, J. C. G. Esteves da Silva and D. Huppert, *J. Phys. Chem. A*, 2018, **122**, 6166–6175.
33 O. Gajst, L. Pinto da Silva, J. C. G. Esteves da Silva and D. Huppert, *J. Phys. Chem. A*, 2018, **122**, 4704–4716.
34 O. Gajst, L. Pinto da Silva, J. C. G. Esteves da Silva and D. Huppert, *J. Phys. Chem. A*, 2019, **123**, 48–58.
35 R. Simkovitch, S. Shomer, R. Gepshtein, M. E. Roth, D. Shabat and D. Huppert, *J. Photochem. Photobiol., A*, 2014, **277**, 90–101.
36 O. Gajst, O. Green, R. Simkovitch, D. Shabat and D. Huppert, *J. Photochem. Photobiol., A*, 2018, **353**, 546–556.
37 I. V. Gopich, K. M. Solntsev and N. Agmon, *J. Chem. Phys.*, 1999, **110**, 2164–2174.
38 L. M. Tolbert and J. E. Haubrich, *J. Am. Chem. Soc.*, 1990, **112**, 8163–8165.
39 L. M. Tolbert and J. E. Haubrich, *J. Am. Chem. Soc.*, 1994, **116**, 10593–10600.
40 L. M. Tolbert and K. M. Solntsev, *Acc. Chem. Res.*, 2002, **35**, 19–27.
41 T. G. Kim and M. R. Topp, *J. Phys. Chem. A*, 2004, **108**, 10060–10065.
42 J. L. Pérez-Lustres, F. Rodriguez-Prieto, M. Mosquera, T. A. Senyushkina, N. P. Ernsting and S. A. Kovalenko, *J. Am. Chem. Soc.*, 2007, **129**, 5408–5418.
43 M. Veiga-Gutiérrez, A. Brenlla, C. Carreira Blanco, B. Fernández, S. A. Kovalenko, F. Rodríguez-Prieto, M. Mosquera and J. L. P. Lustres, *J. Phys. Chem. B*, 2013, **117**, 14065–14078.
44 K. M. Solntsev, C. E. Clower, L. M. Tolbert and D. Huppert, *J. Am. Chem. Soc.*, 2005, **127**, 8534–8544.
45 N. Karton-Lifshin, I. Presiado, Y. Erez, R. Gepshtein, D. Shabat and D. Huppert, *J. Phys. Chem. A*, 2012, **116**, 85–92.
46 R. Simkovitch, N. Karton-Lifshin, S. Shomer, D. Shabat and D. Huppert, *J. Phys. Chem. A*, 2013, **117**, 3405–3413.
47 O. Green, R. Simkovitch, L. Pinto da Silva, J. C. G. Esteves da Silva, D. Shabat and D. Huppert, *J. Phys. Chem. A*, 2016, **120**, 6184–6199.
48 L. Pinto da Silva, O. Green, O. Gajst, R. Simkovitch, D. Shabat, J. C. G. Esteves da Silva and D. Huppert, *ACS Omega*, 2018, **3**, 2058–2073.
49 O. Green, O. Gajst, R. Simkovitch, D. Shabat and D. Huppert, *J. Photochem. Photobiol., A*, 2017, **349**, 230–237.
50 O. Green, O. Gajst, R. Simkovitch, D. Shabat and D. Huppert, *J. Phys. Chem. A*, 2017, **121**, 3079–3087.
51 T. Kumpulainen, B. H. Bakker, M. Hilbers and A. M. Brouwer, *J. Phys. Chem. B*, 2015, **119**, 2515–2524.
52 T. Kumpulainen, B. H. Bakker and A. M. Brouwer, *Phys. Chem. Chem. Phys.*, 2015, **17**, 20715–20724.
53 T. Kumpulainen, A. Rosspeintner, B. Dereka and E. Vauthey, *J. Phys. Chem. Lett.*, 2017, **8**, 4516–4521.
54 P. Verma, A. Rosspeintner, B. Dereka, E. Vauthey and T. Kumpulainen, *Chem. Sci.*, 2020, **11**, 7963–7971.
55 B. Finkler, C. Spies, M. Vester, F. Walte, K. Omlor, I. Riemann, M. Zimmer, F. Stracke, M. Gerhards and G. Jung, *Photochem. Photobiol. Sci.*, 2014, **13**, 548.
56 C. Spies, B. Finkler, N. Acar and G. Jung, *Phys. Chem. Chem. Phys.*, 2013, **15**, 19893.
57 C. Spies, S. Shomer, B. Finkler, D. Pines, E. Pines, G. Jung and D. Huppert, *Phys. Chem. Chem. Phys.*, 2014, **16**, 9104.
58 A. Grandjean, J. L. Pérez Lustres, S. Muth, D. Maus and G. Jung, *J. Phys. Chem. Lett.*, 2021, **12**, 1683–1689.
59 A. Grandjean, J. L. Pérez Lustres and G. Jung, *ChemPhotoChem*, 2021, **5**, 1094–1105.
60 N. Sülzner, B. Geissler, A. Grandjean, G. Jung and P. Nuernberger, *ChemPhotoChem*, 2022, **6**, e202200041.
61 J. Knorr, N. Sülzner, B. Geissler, C. Spies, A. Grandjean, R. J. Kutta, G. Jung and P. Nuernberger, *Photochem. Photobiol. Sci.*, 2022, **21**, 2179–2192.
62 N. Sülzner and C. Hättig, *J. Phys. Chem. A*, 2022, **126**, 5911–5923.
63 A. Klamt, *J. Phys. Chem.*, 1995, **99**, 2224–2235.
64 A. Klamt, V. Jonas, T. Bürger and J. C. W. Lohrenz, *J. Phys. Chem. A*, 1998, **102**, 5074–5085.
65 F. Eckert and A. Klamt, *AIChE J.*, 2002, **48**, 369–385.

66 A. Klamt, *Wiley Interdiscip. Rev.: Comput. Mol. Sci.*, 2011, **1**, 699–709.
67 A. Klamt and G. Schüürmann, *J. Chem. Soc., Perkin Trans. 2*, 1993, 799–805.
68 A. Schäfer, A. Klamt, D. Sattel, J. C. W. Lohrenz and F. Eckert, *Phys. Chem. Chem. Phys.*, 2000, **2**, 2187–2193.
69 F. Siddique, C. P. Silva, G. T. M. Silva, H. Lischka, F. H. Quina and A. J. A. Aquino, *Photochem. Photobiol. Sci.*, 2019, **18**, 45–53.
70 C. P. Silva, G. T. M. Silva, T. D. S. Costa, V. M. T. Carneiro, F. Siddique, A. J. A. Aquino, A. A. Freitas, J. A. Clark, E. M. Espinoza, V. I. Vullev and F. H. Quina, *Pure Appl. Chem.*, 2020, **92**, 255–263.
71 J. Wang, F. Siddique, A. A. Freitas, C. P. Silva, G. T. M. Silva, F. H. Quina, H. Lischka and A. J. A. Aquino, *Theor. Chem. Acc.*, 2020, **139**, 117.
72 J. He, X. Li, G. T. M. Silva, F. H. Quina and A. J. A. Aquino, *J. Braz. Chem. Soc.*, 2019, **30**, 492–498.
73 G. T. M. Silva, C. P. Silva, K. M. Silva, R. M. Pioli, T. S. Costa, V. V. Marto, A. A. Freitas, J. Rozendo, L. M. O. S. Martins, V. F. Cavalcante, L. Sun, A. J. A. Aquino, V. M. T. Carneiro and F. H. Quina, *Photochem*, 2022, **2**, 423–434.
74 D. Jacquemin, E. A. Perpète, I. Ciofini and C. Adamo, *J. Phys. Chem. A*, 2008, **112**, 794–796.
75 T. Le Bahers, C. Adamo and I. Ciofini, *J. Phys. Chem. A*, 2010, **114**, 5932–5939.
76 M. S. Baranov, K. A. Lukyanov, A. O. Borissova, J. Shamir, D. Kosenkov, L. V. Slipchenko, L. M. Tolbert, I. V. Yampolsky and K. M. Solntsev, *J. Am. Chem. Soc.*, 2012, **134**, 6025–6032.
77 É. Brémond, M. E. Alberto, N. Russo, G. Ricci, I. Ciofini and C. Adamo, *Phys. Chem. Chem. Phys.*, 2013, **15**, 10019.
78 Y. Houari, D. Jacquemin and A. D. Laurent, *Phys. Chem. Chem. Phys.*, 2013, **15**, 11875.
79 Y. Houari, D. Jacquemin and A. D. Laurent, *Chem. Phys. Lett.*, 2013, **583**, 218–221.
80 A. Aqdas, F. Siddique, R. Nieman, F. H. Quina and A. J. A. Aquino, *Photochem. Photobiol.*, 2019, **95**, 1339–1344.
81 J. Cui, F. Siddique, R. Nieman, G. T. M. Silva, F. H. Quina and A. J. A. Aquino, *Theor. Chem. Acc.*, 2021, **140**, 90.
82 N. Sülzner, J. Haberhauer, C. Hättig and A. Hellweg, *J. Comput. Chem.*, 2022, **43**, 1011–1022.
83 TURBOMOLE V7.6 2021, a development of University of Karlsruhe and Forschungszentrum Karlsruhe GmbH, 1989–2007, TURBOMOLE GmbH, since 2007; available from **https://www.turbomole.org**.
84 S. G. Balasubramani, G. P. Chen, S. Coriani, M. Diedenhofen, M. S. Frank, Y. J. Franzke, F. Furche, R. Grotjahn, M. E. Harding, C. Hättig, A. Hellweg, B. Helmich-Paris, C. Holzer, U. Huniar, M. Kaupp, A. Marefat Khah, S. Karbalaei Khani, T. Müller, F. Mack, B. D. Nguyen, S. M. Parker, E. Perlt, D. Rappoport, K. Reiter, S. Roy, M. Rückert, G. Schmitz, M. Sierka, E. Tapavicza, D. P. Tew, C. van Wüllen, V. K. Voora, F. Weigend, A. Wodyński and J. M. Yu, *J. Chem. Phys.*, 2020, **152**, 184107.
85 T. Schwabe, K. Sneskov, J. M. Haugaard Olsen, J. Kongsted, O. Christiansen and C. Hättig, *J. Chem. Theory Comput.*, 2012, **8**, 3274–3283.
86 S. Karbalaei Khani, A. Marefat Khah and C. Hättig, *J. Chem. Theory Comput.*, 2020, **16**, 4554–4564.
87 N. Sülzner and C. Hättig, *Zenodo*, 2023, DOI: **10.5281/zenodo.7594763**.
88 T. H. Dunning, *J. Chem. Phys.*, 1989, **90**, 1007–1023.
89 D. E. Woon and T. H. Dunning, *J. Chem. Phys.*, 1993, **98**, 1358–1371.
90 F. Weigend and M. Häser, *Theor. Chem. Acc.*, 1997, **97**, 331–340.
91 C. Hättig, A. Hellweg and A. Köhn, *Phys. Chem. Chem. Phys.*, 2006, **8**, 1159–1169.
92 C. Hättig, *J. Chem. Phys.*, 2003, **118**, 7751–7761.
93 R. Cammi, B. Mennucci and J. Tomasi, *J. Phys. Chem. A*, 1999, **103**, 9100–9108.
94 S. K. Khani, A. M. Khah and C. Hättig, *Phys. Chem. Chem. Phys.*, 2018, **20**, 16354–16363.
95 A. Köhn and C. Hättig, *J. Chem. Phys.*, 2003, **119**, 5021–5036.
96 N. Sülzner and C. Hättig, *Zenodo*, 2022, DOI: **10.5281/zenodo.6598713**.
97 R. A. Kendall, T. H. Dunning and R. J. Harrison, *J. Chem. Phys.*, 1992, **96**, 6796–6806.
98 C. Hättig, in *Advances in Quantum Chemistry*, Academic Press, 2005, vol. 50, pp. 37–60.
99 C. Hättig and F. Weigend, *J. Chem. Phys.*, 2000, **113**, 5154–5161.
100 BIOVIA COSMO*therm*, Release 2021, Dassault Systèmes, **https://www.3ds.com**.
101 A. Klamt, F. Eckert and W. Arlt, *Annu. Rev. Chem. Biomol. Eng.*, 2010, **1**, 101–122.
102 A. Hellweg and F. Eckert, *AIChE J.*, 2017, **63**, 3944–3954.
103 A. Klamt, F. Eckert, M. Diedenhofen and M. E. Beck, *J. Phys. Chem. A*, 2003, **107**, 9380–9386.
104 F. Eckert and A. Klamt, *J. Comput. Chem.*, 2006, **27**, 11–19.
105 F. Eckert, I. Leito, I. Kaljurand, A. Kütt, A. Klamt and M. Diedenhofen, *J. Comput. Chem.*, 2009, **30**, 799–810.
106 P.-F. Loos, F. Lipparini, M. Boggio-Pasqua, A. Scemama and D. Jacquemin, *J. Chem. Theory Comput.*, 2020, **16**, 1711–1741.
107 M. R. Silva-Junior, S. P. Sauer, M. Schreiber and W. Thiel, *Mol. Phys.*, 2010, **108**, 453–465.
108 M. Schreiber, M. R. Silva-Junior, S. P. A. Sauer and W. Thiel, *J. Chem. Phys.*, 2008, **128**, 134110.
109 M. J. Kamlet, J. L. M. Abboud, M. H. Abraham and R. W. Taft, *J. Org. Chem.*, 1983, **48**, 2877–2887.
110 P. F. McGarry, S. Jockusch, Y. Fujiwara, N. A. Kaprinidis and N. J. Turro, *J. Phys. Chem. A*, 1997, **101**, 764–767.
111 Z. Yuan, Q. Tang, K. Sreenath, J. T. Simmons, A. H. Younes, D.-E. Jiang and L. Zhu, *Photochem. Photobiol.*, 2015, **91**, 586–598.
112 S. Wortmann, S. Schloeglmann and P. Nuernberger, *J. Org. Chem.*, 2022, **87**, 1745–1755.
113 G. Akerlof, *J. Am. Chem. Soc.*, 1932, **54**, 4125–4139.

This journal is © the Owner Societies 2023